Cross-Domain Multicarrier Waveform Design for Integrated Sensing and Communication

Fan Zhang[1], Tianqi Mao[2], Ruiqi Liu[3], Zhu Han[4], *Fellow, IEEE*, Octavia A. Dobre[5], *Fellow, IEEE*, Sheng Chen[6], *Life Fellow, IEEE*, and Zhaocheng Wang[1], *Fellow, IEEE*,

[1]Department of Electronic Engineering, Tsinghua University, Beijing 100080, China

[2]Advanced Research Institute of Multidisciplinary Science, Beijing Institute of Technology, Beijing 100081, China

[3] Wireless and Computing Research Institute, ZTE Corporation, Beijing 100029, China

[4] Department of Electrical and Computer Engineering, University of Houston, Houston, TX 77004, USA

[5] Faculty of Engineering and Applied Science, Memorial University, St. John's, NL A1C 5S7, Canada

[6] School of Electronics and Computer Science, University of Southampton, Southampton SO17 1BJ, U.K.

***Abstract*—Integrated sensing and communication (ISAC) is expected to be a promising technology in the sixth-generation (6G) wireless networks for its ability to alleviate resources shortage and excessive hardware expenses. One typical representative for ISAC waveforms is the orthogonal frequency division multiplexing (OFDM) waveform, which divides the time-frequency resources into orthogonal resource elements (REs). In order to satisfy their diverse design requirements and mitigate mutual interference, the communication and sensing subsystems can be assigned with different REs, which necessitates effective allocation strategies of different resources across time and frequency domains. In this article, a cross-domain multicarrier waveform design methodology is proposed, which optimizes the RE assignment and power allocation strategies for the OFDM-based ISAC system. Specifically, for sensing performance enhancement, the unit cells of the ambiguity function (AF) of the sensing components are specially shaped to achieve a "locally" perfect auto-correlation (AC) property within a predefined region of interest (RoI) in the Delay-Doppler domain. Afterwards, the irrelevant cells outside the RoI, which can determine the sensing power allocation strategy, are optimized alternatively with the communication power allocation strategy to maximize the throughput for the communication purpose. Numerical results demonstrate the superiority of the cross-domain multicarrier waveform design, which also provides useful guidelines for parameter settings of the proposed OFDM-based ISAC system.**

I. Introduction

The unprecedented advancements of digital signal processing in recent years have prompted the convergence of communication and sensing systems regarding transceiver structure and frequency resources, which yields the emerging integrated sensing and communication (ISAC) technology [1]–[3]. By sharing the hardware platform and spectrum resources, the ISAC system can enable simultaneous data transmission and target detection with low hardware complexity and high spectrum efficiency. Additionally, it allows the mutual information exchange for further performance enhancement of the dual subsystems [4]. Thanks to these advantages, ISAC systems have facilitated a plethora of cutting-edge applications, including intelligent transportation and virtual reality [5].

Orthogonal frequency division multiplexing (OFDM), as one representative ISAC waveform, boasts the robustness against frequency-selective fading. In contrast to single-carrier waveforms, which can only allocate resources in the time domain, OFDM operates within a two-dimensional space, encompassing both time and frequency domains [6]. This unique characteristic endows OFDM with increased flexibility for radar sequence design and processing. In order to satisfy the distinct design requirements of communication and sensing, as well as avoid the potential interference between them, an OFDM-based ISAC waveform with interleaved subcarriers, abbreviated as OFDM-IS, was proposed in [7], where the communication and sensing subsystems are assigned with orthogonal time-frequency resources. In OFDM-IS-based ISAC systems, the optimization design of the RE and power allocation is significant for sensing and communication performance enhancement.

Against this background, a comprehensive optimization was performed on OFDM subcarrier assignment and power allocation within ISAC systems in [7], with the primary goal of improving the compound mutual information (MI) of sensing and communication subsystems. Furthermore, in [8], an additional strategy was introduced, aiming to minimize overall power consumption while adhering to constraints on both the sensing MI metric and the communication data rate. Meanwhile, [9] allocated the subcarrier and power to maximize the peak-to-sidelobe ratio (PSLR) in the radar range profile while maintaining an acceptable level of the communication throughput. All of the aforementioned studies only focused on the optimization of resource allocation within one single OFDM symbol. However, to improve the speed resolution in radar sensing, the processing interval usually has to be extended by incorporating multiple consecutive OFDM symbols. Consequently, to enhance both sensing and communication performance across relatively long time intervals, optimization of the ISAC waveform design across multiple consecutive OFDM symbols is necessary, where the existing attempts are still at their infancy.

Following this philosophy, a cross-domain multicarrier waveform design methodology is developed, which optimizes the RE assignment and power allocation in both time and frequency domains. The contributions of this paper can be summarized as follows:

- To preserve a "locally" perfect auto-correlation (AC) property while maintaining an acceptable communication data rate, the integrated waveform design is formulated as

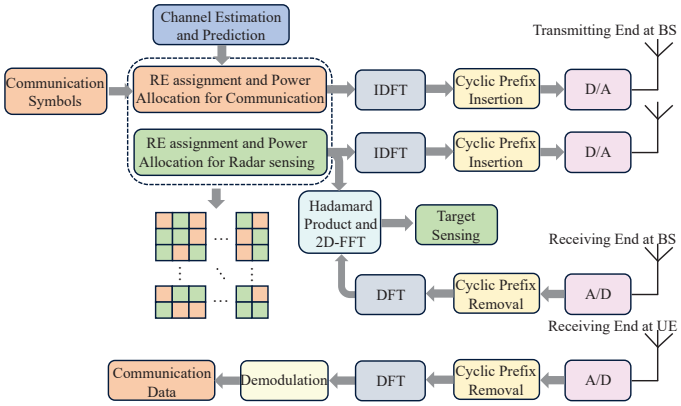

Fig. 1. Transceiver structure of OFDM-IS-based ISAC systems.

an optimization problem, which involves both the time-frequency domain and the Delay-Doppler domain.

- Afterwards, a low-complexity alternating iterative algorithm is proposed, where the irrelevant cells in the Delay-Doppler domain and the communication power allocation in the time-frequency domain are optimized alternatively to maximize the communication data rate.

Numerical results show that the proposed cross-domain waveform design methodology maintains a "locally" perfect AC property within the RoI while achieving a quasi-maximal data rate.

Notation: DFT$(\mathbf{X}, i)$ and IDFT$(\mathbf{X}, i)$ denote performing discrete Fourier transformation (DFT) and inverse DFT (IDFT) along the i-th dimension of the matrix $\mathbf{X}$, respectively. $(\mathbf{X})^{\mathrm{T}}$ and $(\mathbf{X})^{*}$ stands for the transpose and conjugate of $\mathbf{X}$. $\mathbf{1}$ denotes the all-one matrix. $|\mathbf{X}|^2$ is a matrix that contains the element-wise absolute square value of $\mathbf{X}$, and $||\mathbf{X}||$ denotes the Frobenius norm of the matrix $\mathbf{X}$. For a matrix $\mathbf{X}$, $X(m,k)$ denotes its element in the m-th row and the k-th column.

II. System Model

In this paper, a mono-static ISAC system is considered, where a base station (BS) transmits data to user equipment (UE) while simultaneously scanning different directions with probing signals for target sensing. In order to ensure high array gain, large-scale antenna arrays are employed to form directional beams, which is approximately equivalent to a single directional antenna. Therefore, for simplicity, we assume single-input single-output (SISO) systems for both communications and sensing.

A. Transmitted Signal Model

The OFDM-IS-based waveform is utilized for simultaneous target sensing and data transmission, where the transceiver structure is illustrated in Fig. 1. Specifically, a transmit frame of M consecutive OFDM symbols with K subcarriers is considered and the k-th subcarrier in the m-th symbol is referred to as the (m,k)-th RE, abbreviated as RE$_{m,k}$. We employ the matrix $\mathbf{U} \in \mathbb{Z}^{M\times K}$ to indicate whether REs are selected for sensing or communications, written as

$$U(m,k) = \begin{cases} 1, & \text{if RE}_{m,k} \text{ is for sensing,} \\ 0, & \text{if it is for communications.} \end{cases} \tag{1}$$

Let $\mathbf{X} \in \mathbb{C}^{M\times K}$ denote the transmit signal matrix with $X(m,k)$ representing the modulated symbol in RE$_{m,k}$. Then the sensing and communication transmit signal matrices $\mathbf{X}_{\mathrm{r}} \in \mathbb{C}^{M\times K}$ and $\mathbf{X}_{\mathrm{c}} \in \mathbb{C}^{M\times K}$, can be expressed as $\mathbf{X}_{\mathrm{r}} = \mathbf{U} \odot \mathbf{X}$ and $\mathbf{X}_{\mathrm{c}} = (\mathbf{1} - \mathbf{U}) \odot \mathbf{X}$, respectively, where $\odot$ represents the Hadamard product. Afterwards, by performing IDFT on $\mathbf{X}_{\mathrm{r}}$ and $\mathbf{X}_{\mathrm{c}}$, the time-domain transmit signals in a discrete form can be derived as

$$x_{\mathrm{i}}[n] = \frac{1}{\sqrt{K}} \sum_{m=0}^{M-1} \sum_{k=0}^{K-1} X_{\mathrm{i}}(m,k)\, e^{\mathrm{j}2\pi \frac{k(n-mK)}{K}} \mathrm{rect}\left(\frac{n-mK}{K}\right), \tag{2}$$

with $n = 0, 1, \cdots, MK-1$, where $\mathrm{i} = \mathrm{r}$ represents the sensing sequence and $\mathrm{i} = \mathrm{c}$ represents the communication sequence. Besides, rect(t) is a rectangle function, which equals 1 when $0 \le t < 1$ and equals 0 otherwise. Before transmission, the cyclic prefix with length T_{G} is inserted in front of each OFDM symbol, making its total duration equal to $T_{\mathrm{O}} = T + T_{\mathrm{G}}$. Finally, the discrete signals are converted to analog signals by a digital-to-analog converter (D/A) and transmitted to UE.

B. Received Signal Model for Communications

After analog-to-digital (A/D) conversion, CP removal, and DFT operation, the communication received matrix $\mathbf{Y}_{\mathrm{c}} \in \mathbb{C}^{M\times K}$ is obtained as

$$\mathbf{Y}_{\mathrm{c}} = \mathbf{H} \odot \mathbf{X}_{\mathrm{c}} + \mathbf{W}_{\mathrm{c}}, \tag{3}$$

where $\mathbf{H} \in \mathbb{C}^{M\times K}$ denotes the channel coefficient matrix and $\mathbf{W}_{\mathrm{c}}$ is the matrix representation of the additive white Gaussian noise (AWGN) with $W_{\mathrm{c}}(m,k) \sim \mathcal{CN}(0, \sigma_{\mathrm{c}}^2)$. Considering both the multi-path and Doppler shift effects for data transmission, the channel matrix $\mathbf{H}$ can be expressed as [10]

$$H(m,k) = \sum_{l=1}^{L} \alpha_l e^{\mathrm{j}2\pi(v_l m T_O - \tau_l k \Delta f)}. \tag{4}$$

Here L is the number of paths, and v_l, τ_l and α_l denote the Doppler shift, delay and complex gain on the l-th path, respectively. For simplicity, the communication channel $\mathbf{H}$ within M OFDM symbols is assumed to be perfectly estimated in this paper.

C. Received Signal Model for Sensing

By denoting the distance and relative radial speed of the target as s and v, respectively, the received echoes $y_{\mathrm{r}}[n]$ can be written as

$$y_{\mathrm{r}}[n] = x_{\mathrm{r}}\left[n - \left\lfloor \frac{2s}{cT_{\mathrm{s}}} \right\rfloor\right] e^{\mathrm{j}\left(2\pi n \frac{2v f_{\mathrm{c}} T_{\mathrm{s}}}{c}\right)} + w_{\mathrm{r}}[n], \tag{5}$$

where T_s represents the sampling period and $w_{\mathrm{r}}[n] \sim \mathcal{CN}(0, \sigma_{\mathrm{r}}^2)$ denotes the thermal noise plus the clutters from other directions. By performing DFT on each K-length segment of $y_{\mathrm{r}}[n]$ sequentially and then converting the serial results to parallel form, the sensing received signal matrix $\mathbf{Y}_{\mathrm{r}} \in \mathbb{C}^{M\times K}$ can be obtained as

$$Y_{\mathrm{r}}(m,k) = \sum_{n=(m-1)K}^{mK-1} y_{\mathrm{r}}[n] e^{\mathrm{j}2\pi \frac{(n-(m-1)K)k}{K}}. \tag{6}$$

Assuming that the time delay of the target is shorter than T_{G}, the range-Doppler matrix can be generated by performing DFT and IDFT on the Hadamard product of $(\mathbf{X}_{\mathrm{r}})^*$ and $\mathbf{Y}_{\mathrm{r}}$, which can be expressed as

$$\mathbf{R} = \mathrm{DFT}(\mathrm{IDFT}((\mathbf{X}_{\mathrm{r}})^* \odot \mathbf{Y}_{\mathrm{r}}, 1), 2), \tag{7}$$

and can be employed for target sensing via hypothesis tests. The readers are referred to [11] for more details about the sensing algorithm.

III. Proposed Cross-Domain ISAC Waveform Design

In this section, the relationship between the AF in the Delay-Doppler domain and the sensing power allocation in the time-frequency domain is firstly revealed. Afterwards, to attain an acceptable throughput level while maintaining a "locally" perfect AC property within a predefined RoI, the Delay-Doppler domain AF coefficients and the power allocation strategy for communications are jointly designed by solving an optimization problem in an alternating iterative manner.

A. Problem Formulation

The AF is a crucial performance metric for sensing sequences, which is defined as their two-dimensional autocorrelation results in the Delay-Doppler domain. Specifically, the AF of an N-length sensing sequence $s[n]$ can be expressed as

$$\Phi(\tau,\nu) = \sum_{n=0}^{N-1} s[n]s^*[n+\tau]e^{\mathrm{j}2\pi\nu n/N}, \tag{8}$$

where $\tau = 0, 1, \cdots, N-1$ and $\nu = 0, 1, \cdots, N-1$ denote the delay and Doppler indices, respectively. By substituting (2) into (8), the AF of the OFDM-based sensing sequence can be derived as

$$\begin{aligned}\Phi(\tau,\nu) = &\sum_{n=0}^{MK-1}\left(\sum_{m_1=0}^{M-1}\sum_{k_1=0}^{K-1} X_{\mathrm{r}}(m_1,k_1)\,\psi(n,m_1,k_1)\right)\\ &\times\left(\sum_{m_2=0}^{M-1}\sum_{k_2=0}^{K-1} X_{\mathrm{r}}^*(m_2,k_2)\psi(n+\tau,m_2,k_2)\right)e^{\mathrm{j}2\pi\frac{\nu n}{MK}},\end{aligned} \tag{9}$$

where $\psi(n,m,k) = e^{\mathrm{j}2\pi k(n-mK)/K}\mathrm{rect}\left(\frac{n-mK}{K}\right)$. Due to the cyclic prefix protection and the orthogonality of subcarriers, we neglect the inter-symbol ($m_1 \neq m_2$) and inter-subcarrier ($k_1 \neq k_2$) interference. Therefore, the AF of the waveform can be approximated as follows:

$$\Phi(\tau,\nu)\approx\left(\sum_{m=0}^{M-1}\sum_{k=0}^{K-1} P_{\mathrm{r}}(m,k)\,e^{-\mathrm{j}2\pi\frac{\tau k}{K}}e^{\mathrm{j}2\pi\frac{\nu m}{M}}\right)b(\nu), \tag{10}$$

where $P_{\mathrm{r}}(m,k) = |X_{\mathrm{r}}(m,k)|^2$ is the sensing power allocated on the $\mathrm{RE}_{m,k}$. Besides, $b(\nu)$ denotes $\sum_{n=0}^{K-1} e^{\mathrm{j}2\pi\frac{\nu n}{MK}}$, which is independent of the sensing sequence and thus considered as a linear coefficient. Note that $\Phi(\tau,\nu)$ reaches its maximum when τ and μ are multiples of K and M, respectively. Therefore, to avoid the ambiguity problem in target sensing, we usually consider the principal interval (PI) of the AF as the region $(\tau,\nu) \in \Pi = \left[-\left\lfloor\frac{K}{2}\right\rfloor, -\left\lfloor\frac{K}{2}\right\rfloor+1, \cdots, K-1-\left\lfloor\frac{K}{2}\right\rfloor\right] \times \left[-\left\lfloor\frac{M}{2}\right\rfloor, -\left\lfloor\frac{M}{2}\right\rfloor+1, \cdots, M-1-\left\lfloor\frac{M}{2}\right\rfloor\right]$ [6]. Furthermore, since practical sensing applications usually concern specific scopes of the target distance and speed rather than the entire PI, we mainly focus on the sensing performance within an RoI in the Delay-Doppler domain, written as

$$\begin{aligned}\Pi_{\mathrm{s}} = &\left[0, 1, 2\cdots, \frac{K}{p}-1-\left\lfloor\frac{K}{2p}\right\rfloor\right]\\ &\times\left[-\left\lfloor\frac{M}{2q}\right\rfloor, -\left\lfloor\frac{M}{2q}\right\rfloor+1, \cdots, \frac{M}{q}-1-\left\lfloor\frac{M}{2q}\right\rfloor\right],\end{aligned} \tag{11}$$

where p and q are factors of K and M, respectively. Note that the corresponding sensing scopes of distance and speed for Π_{s} are $\left[0, \frac{c}{2p\Delta f}\right)$ and $\left(\frac{c}{4qf_cT_{\mathrm{O}}}, \frac{c}{4qf_cT_{\mathrm{O}}}\right)$, respectively. If the required sensing scopes of distance and speed are set as $[0, s_0]$ and $[-v_0, v_0]$, respectively, p and q should be selected as the maximum factors of K and M, respectively, such that $\left[0, \frac{c}{2p\Delta f}\right)$ and $\left(\frac{c}{4qf_cT_{\mathrm{O}}}, \frac{c}{4qf_cT_{\mathrm{O}}}\right)$ contain $[0, s_0]$ and $[-v_0, v_0]$, respectively.

Following this philosophy, the "locally" perfect AC property of the sensing component is readily constructed to ensure accurate sensing through the manipulation of the AF coefficients within the RoI, expressed as

$$\Phi(\tau,\nu) = \begin{cases} Kp_{\mathrm{r}}^{\mathrm{t}}, & (\tau,\nu) = (0,0),\\ 0, & (0,0) \neq (\tau,\nu) \in \Pi_{\mathrm{s}},\end{cases} \tag{12}$$

where $p_{\mathrm{r}}^{\mathrm{t}}$ is the total sensing power. On the other hand, according to (10), since $\Phi(\tau,\nu)$ can be derived by performing DFT and IDFT on $P_{\mathrm{r}}(m,k)$ and multiplying it with $b(\nu)$, $P_{\mathrm{r}}(m,k)$ can be calculated by performing the inverse transformation on $\Phi(\tau,\nu)$ as

$$P_{\mathrm{r}}(m,k) = \frac{1}{MK}\sum_{\nu=-\lfloor M/2\rfloor}^{M-1-\lfloor M/2\rfloor}\sum_{\tau=-\lfloor K/2\rfloor}^{K-1-\lfloor K/2\rfloor}\frac{\Phi(\tau,\nu)}{b(\nu)}e^{\mathrm{j}2\pi\frac{\tau k}{K}}e^{-\mathrm{j}2\pi\frac{\nu m}{M}}. \tag{13}$$

It can be seen from (12) and (13) that, to guarantee "locally" perfect AC property, the AF values of the unit cells within Π_{s} should be constant, while the cells outsides Π_{s} (referred to as "irrelevant cells" below) can be manipulated to determine the power allocation pattern for sensing.

Specifically, we denote the complementary set of Π_{s} in Π as $\bar{\Pi}_{\mathrm{s}}$. Then, the irrelevant cells of the AF within $\bar{\Pi}_{\mathrm{s}}$ are specially designed to guarantee non-negative real values for $P_{\mathrm{r}}(m,k)$, which can be formulated as

$$\begin{aligned}\text{find}\quad &\Phi(\tau,\nu),\ \text{for}\ (\tau,\nu) \in \bar{\Pi}_{\mathrm{s}},\\ \text{s.t.}\quad &P_{\mathrm{r}}(m,k) \geq 0,\ P_{\mathrm{r}}(m,k) = P_r^*(m,k),\end{aligned} \tag{14}$$

which necessitates centro-hermitian symmetry for $\Phi(\tau,\nu)$ according to (15), i.e., $\Phi(\tau,\nu) = \Phi^*(-\tau,-\nu)$. This inspires us to further reduce the dimension of the optimization variable. To be more specific, as shown in Fig. 2, the entire region Π is partitioned into upper and lower parts by the ν-axis. As the two parts are mutually centro symmetric, it is only necessary to design the values of unit cells in the upper part, denoted as $\Pi_{\mathrm{r}} = \left[-\lfloor M/2\rfloor, \cdots, M-1-\lfloor M/2\rfloor\right] \times \left[0, 1, \cdots, K-1-\lfloor K/2\rfloor\right]$. Besides, Π_r consists of the RoI Π_{s} and the outer region

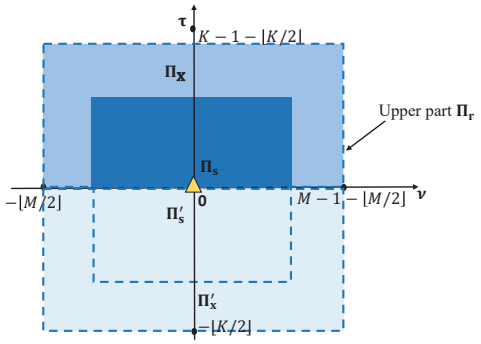

Fig. 2. Different regions in the Delay-Doppler domain.

Π_{x} as shown in Fig. 2. Since the unit cells in Π_{s} have already determined to ensure the perfect AC property, only the ambiguity values in Π_{x} require consideration to ensure unipolar values for $P_r(m,k)$, written as

$$\begin{aligned} \text{find} \quad & \Phi(\tau,\nu), \ \text{for} \ (\tau,\nu)\in\Pi_{\mathrm{x}}, \\ \text{s.t.} \quad & P_{\mathrm{r}}(m,k)\geq 0. \end{aligned} \tag{15}$$

For different feasible power allocation strategies of sensing applications, the REs with low allocated sensing power, i.e., lower than a predefined threshold ϵ, are considered to pose marginal impact on the sensing performance. Therefore, such REs are employed for the communication subsystem, and the matrix $\mathbf{U}$ can be expressed as

$$U(m,k)=\begin{cases} 1, & \text{if } P_{\mathrm{r}}(m,k)>\epsilon, \\ 0, & \text{if } P_{\mathrm{r}}(m,k)\leq\epsilon. \end{cases} \tag{16}$$

Finally, the communication power allocation strategy for such REs are optimized for data rate enhancement. Based on the aforementioned operations, a joint optimization problem is established to maximize the communication data rate among different solutions of (15), formulated as

$$\begin{aligned} \max_{\Phi(\tau,\nu),\mathbf{P}_{\mathrm{c}}} \quad & \sum_{m=0}^{M-1}\sum_{k=0}^{K-1}\log\Big(1+\tfrac{(1-U(m,k))P_{\mathrm{c}}(m,k)|H(m,k)|^2}{\sigma_{\mathrm{c}}^2}\Big), \\ \text{s.t.} \quad & P_{\mathrm{r}}(m,k)\geq 0, \\ & \sum_{m=0}^{M-1}\sum_{k=0}^{K-1}P_{\mathrm{c}}(m,k)=p_{\mathrm{c}}^{\mathrm{t}}, \ P_{\mathrm{c}}(m,k)\geq 0, \end{aligned} \tag{17}$$

where $p_{\mathrm{c}}^{\mathrm{t}}$ denotes the total communication power. Problem (17) can be solved by exhaustively searching for the values of $\Phi(\tau,\nu)$ within Π_{x}, which induces considerable computational complexity. In the following, a low-complexity alternating iterative algorithm is proposed to solve problem (17) with a quasi-optimal solution.

B. Proposed Low-Complexity Alternating Iterative Algorithm

Problem (17) can be naturally divided into two sub-problems: the irrelevant cell design of the AF and the communication power allocation, corresponding to the optimization of $\Phi(\tau,\nu)$ and $\mathbf{P}_{\mathrm{c}}$, respectively. This inspires us to optimize these dual variables in an alternating iterative manner, which is shown as Algorithm 1. Before we proceed, we denote the optimization variables in the j-th iteration as $\mathbf{P}_{\mathrm{c}}^{(j)}$ and $\Phi^{(j)}(\tau,\nu)$. Accordingly, the sensing power allocation strategy and the indicating matrix in the j-th iteration, denoted as $\mathbf{P}_{\mathrm{r}}^{(j)}$ and $\mathbf{U}^{(j)}$, can be calculated based on $\Phi^{(j)}(\tau,\nu)$ according to (13) and (16). The optimized achievable data rate in the j-th iteration is denoted as $opt^{(j)}$, and the maximum number of iterations is denoted as J_{m}. Below we describe the detailed process of the proposed alternating iterative algorithm.

At the beginning, we initialize $\Phi(\tau,\nu)$ as $\Phi^{(0)}(\tau,\nu)$. Taking the j-th iteration as an example, each iteration consists of the following two stages:

Stage 1. Optimization of $\mathbf{P}_{\mathrm{c}}^{(j)}$*:* The problem can be formulated as

$$\begin{aligned} \max_{\mathbf{P}_{\mathrm{c}}^{(j)}} \quad & \sum_{m=0}^{M-1}\sum_{k=0}^{K-1}\log\Big(1+\tfrac{(1-U^{(j-1)}(m,k))P_{\mathrm{c}}^{(j)}(m,k)|H(m,k)|^2}{\sigma_{\mathrm{c}}^2}\Big) \\ \text{s.t.} \quad & \sum_{m=0}^{M-1}\sum_{k=0}^{K-1}P_{\mathrm{c}}^{(j)}(m,k)=p_{\mathrm{c}}^{\mathrm{t}}, \ \ P_{\mathrm{c}}^{(j)}(m,k)\geq 0. \end{aligned} \tag{18}$$

By applying the Karush-Kuhn-Tucker (KKT) conditions, the optimal solution of sub-problem (18) can be expressed as [12]

$$P_{\mathrm{c}}^{(j)}(m,k)=\begin{cases} \max\left\{\frac{1}{\alpha\ln 2}-\frac{\sigma_{\mathrm{c}}^2}{|H(m,k)|^2},0\right\}, & U^{(j-1)}(m,k)=0, \\ 0, & U^{(j-1)}(m,k)=1. \end{cases} \tag{19}$$

Here $\frac{1}{\alpha\ln 2}=\frac{p_{\mathrm{c}}^{\mathrm{t}}+\sum_{(m,k)\in\mathcal{S}}\frac{\sigma_{\mathrm{c}}^2}{|H(m,k)|^2}}{\mathrm{card}(\mathcal{S})}$, where $\mathcal{S}$ is the set of REs with $P_{\mathrm{c}}^{(j)}(m,k)>0$ and $\mathrm{card}(\mathcal{S})$ is its cardinality.

Stage 2. Optimization of $\Phi(\tau,\nu)^{(j)}$*:* Based on the optimization results of $\mathbf{P}_{\mathrm{c}}^{(j)}$, the irrelevant cell design can be written as

$$\begin{aligned} \max_{\Phi^{(j)}(\tau,\nu)} \quad & \sum_{m=0}^{M-1}\sum_{k=0}^{K-1}\log\Big(1+\tfrac{(1-U^{(j)}(m,k))P_{\mathrm{c}}^{(j)}(m,k)|H(m,k)|^2}{\sigma_{\mathrm{c}}^2}\Big) \\ \text{s.t.} \quad & P_{\mathrm{r}}^{(j)}(m,k)\geq 0. \end{aligned} \tag{20}$$

To solve sub-problem (20), a linear continuous function is employed to approximate the non-convex mapping between $U^{(j)}(m,k)$ and $P_{\mathrm{r}}^{(j)}(m,k)$. Specifically, we use $P_{\mathrm{r}}^{(j)}(m,k)/r_{\mathrm{m}}$ to approximate $U^{(j)}(m,k)$, where r_{m} is a normalization factor of $P_{\mathrm{r}}^{(j)}(m,k)$, set as the largest element of $\mathbf{P}_{\mathrm{r}}^{(0)}$. The approximation is increasingly accurate when $P_{\mathrm{r}}^{(i)}(m,k)$ is close to 0 or r_{m}. Therefore, we incorporate a penalty term $\gamma\left(P_{\mathrm{r}}^{(j)}(m,k)\right)$ into the objective function to indicate how close $P_{\mathrm{r}}^{(j)}(m,k)$ is to 0 or r_{m}, which can be expressed as

$$\gamma\left(P_{\mathrm{r}}^{(j)}(m,k)\right)=-P_{\mathrm{r}}^{(j)}(m,k)\left(1-P_{\mathrm{r}}^{(j)}(m,k)/r_{\mathrm{m}}\right). \tag{21}$$

Then, sub-problem (20) can be re-written as

$$\begin{aligned} \max_{\Phi^{(j)}(\tau,\nu)} \quad & \sum_{m=0}^{M-1}\sum_{k=0}^{K-1}\log\Big(1+\tfrac{\left(1-\frac{P_{\mathrm{r}}^{(j)}(m,k)}{r_{\mathrm{m}}}\right)P_{\mathrm{c}}^{(j)}(m,k)|H(m,k)|^2}{\sigma_{\mathrm{c}}^2}\Big) \\ & +\lambda\gamma\left(P_{\mathrm{r}}^{(j)}(m,k)\right) \\ \text{s.t.} \quad & 0\leq P_{\mathrm{r}}^{(j)}(m,k)\leq r_{\mathrm{m}}, \end{aligned} \tag{22}$$

where λ is a weight factor which strikes a balance between the data rate and the requirement for the range of $P_{\mathrm{r}}^{(j)}(m,k)$.

Algorithm 1 Proposed cross-domain ISAC waveform design

Input: $p_{\mathrm{c}}^{\mathrm{t}}$, $p_{\mathrm{r}}^{\mathrm{t}}$, $\mathbf{H}$, Π_s, J_{m}, I_{m}, δ_1, δ_2

Initialize $\Phi^{(0)}(\tau,\nu)$ by solving problem (24);
Calculate $\mathbf{P}_{\mathrm{r}}^{(0)}$ and $\mathbf{U}^{(0)}$ according to (13) and (16).
while $j \leq J_{\mathrm{m}}$ or $|opt^{(j)} - opt^{(j-1)}| < \delta_1$ **do**
  Calculate $\mathbf{P}_{\mathrm{c}}^{(j)}$ according to problem (18); $j=j+1$;
  while $i \leq I_{\mathrm{m}}$ or $||\mathbf{P}_{\mathrm{r}}^{(j,i)} - \mathbf{P}_{\mathrm{r}}^{(j,i-1)}|| < \delta_2$ **do**
    Calculate $\gamma^{(j,i)}(\mathbf{P}_{\mathrm{r}},\nu,\mu)$, $\mathbf{P}_{\mathrm{r}}^{(j,i)}$ according to problem (23); $i=i+1$;
  end while
  Calculate $\mathbf{U}^{(j)}$ according to (16).
end while
return $\mathbf{U}$, $\mathbf{P}_{\mathrm{r}}$, $\mathbf{P}_{\mathrm{c}}$.

The solution of problem (22) can be still challenging due to its non-concave objective function. To address this issue, we instead employ the Minorize-Maximization (MM) algorithm, where a lower bound of the objective function is derived by converting the second term $\gamma\left(P_{\mathrm{r}}^{(j)}(m,k)\right)$ into its linear approximation. By maximizing the lower bound of the objective function iteratively, the obtained results will finally converge to the optimal solution of the original problem [13]. For simplicity, we denote the optimization variables in the i-th iteration as $\Phi^{(j,i)}(\tau,\nu)$. Accordingly, the sensing power allocation strategy $\mathbf{P}_{\mathrm{r}}^{(j,i)}$ can be calculated with $\Phi^{(j,i)}(\tau,\nu)$ according to (13). The problem in the i-th iteration of the MM algorithm can be written as

$$\begin{aligned}\max_{\Phi^{(j,i)}(\tau,\nu)} \quad & \sum_{m=0}^{M-1}\sum_{k=0}^{K-1} \log\left(1+\frac{(1-\frac{P_{\mathrm{r}}^{(j,i)}(m,k)}{r_{\mathrm{m}}})P_{\mathrm{c}}^{(j)}(m,k)|H(m,k)|^2}{\sigma_{\mathrm{c}}^2}\right) \\ & -\lambda\left(P_{\mathrm{r}}^{(j,i)}(m,k)-\frac{2P_{\mathrm{r}}^{(j,i-1)}(m,k)}{r_{\mathrm{m}}}P_{\mathrm{r}}^{(j,i)}(m,k)\right) \\ \text{s.t.} \quad & 0 \leq P_{\mathrm{r}}^{(j,i)}(m,k) \leq r_{\mathrm{m}}.\end{aligned} \tag{23}$$

When i is larger than the maximum number of iteration I_{m}, or $||\mathbf{P}_{\mathrm{r}}^{(j,i)} - \mathbf{P}_{\mathrm{r}}^{(j,i-1)}||$ is less than a predefined threshold δ_2, the iteration will be terminated and $\Phi^{(j)}(\tau,\nu)$ will be obtained as $\Phi^{(j,i)}(\tau,\nu)$.

Note that the alternating iterative algorithm is a heuristic method, whose convergence is related to the choice of the initial value. To facilitate fast convergence of Algorithm 1 with low computational complexity, an initial value that can be readily obtained whilst approaching the optimal solution is desirable. Following this philosophy, we derive the initial value $\Phi^{(0)}(\tau,\nu)$ by solving the following linear programming problem:

$$\begin{aligned}\min_{\Phi^{(0)}(\tau,\nu)} \quad & \sum_{m=0}^{M-1}\sum_{k=0}^{K-1} P_{\mathrm{r}}^{(0)}(m,k)|H(m,k)|^2 \\ \text{s.t.} \quad & P_{\mathrm{r}}^{(0)}(m,k) \geq 0,\end{aligned} \tag{24}$$

which can be easily solved with low computational complexity. Note that problem (24) aims to allocate lower sensing power to REs with higher communication channel gains, which avoids possible occupation of the high-quality communication channels for sensing.

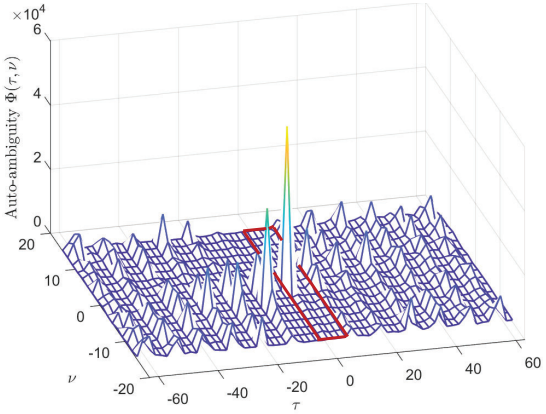

Fig. 3. Ambiguity function of the proposed cross-domain waveform design.

IV. Numerical Results

In this section, an OFDM-IS-based ISAC system is considered, where each coherent processing interval consists of 32 consecutive OFDM symbols with 128 subcarriers. Firstly, the AF pattern of the proposed cross-domain waveform design is illustrated, which validates its "locally" perfect AC property. Afterwards, its communication performance is evaluated in term of the achievable data rate, compared with the communication-only waveform which occupies the entire OFDM frame for data transmission. Moreover, the performance trade-off between sensing and communications is investigated to find the optimal parameter design numerically.

The AF of the sensing sequence derived by our proposed waveform design methodology is presented in Fig. 3. The required sensing scopes of distance and speed are set as $[0, 50]$ m and $[-60, 60]$ m/s, respectively. The corresponding RoI can be calculated according to (11), as outlined with red lines in Fig. 3. Due to the presence of non-negligible sidelobes outside the RoI, the PSLR across the entire AF is less than 1 dB. On the contrary, within the RoI, the level of sidelobes is marginal, which results in a PSLR of over 20 dB, indicating that the proposed waveform boasts a "locally" perfect AC property within the RoI.

Figs. 4(a) and 4(b) illustrate the achievable data rate of the proposed waveform with respect to the sensing scopes of distance and speed, under different ratios of the allocated power between sensing and communications. The baseline, referred to as the 'maximal value', is obtained by optimizing the communication performance in a communication-only system. As observed, the achievable data rates for both our proposed waveform and the baseline increase as the ratio of allocated sensing power to communication power decreases. This is due to the increased allocation of power to the communications. Furthermore, the RoI is increasingly large as the sensing scopes of distance and speed expand, which leads to the decrease in the number of irrelevant cells, i.e., the dimension of optimization variables for communication performance. Therefore, the achievable data rate is degraded slightly when the sensing scopes are relatively large. However, it still closely approaches the maximal value when sensing scopes of distance and speed are no more than 40 m and ± 50 m/s, respectively.

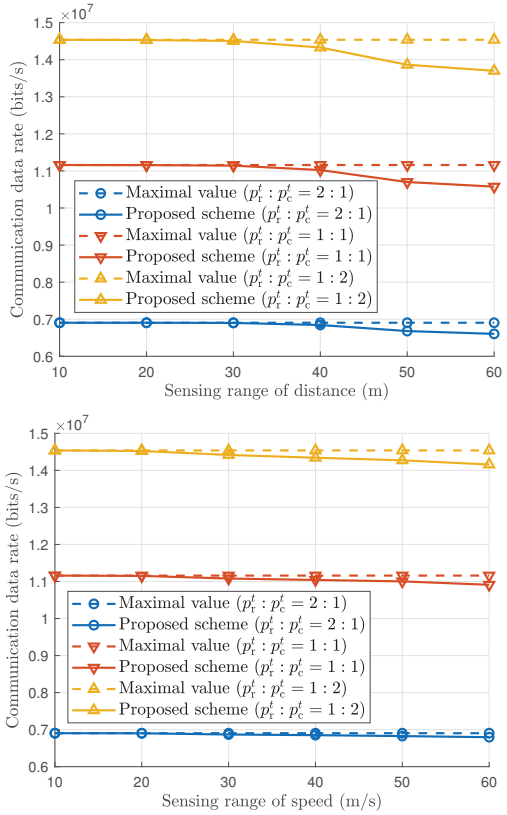

Fig. 4. (a) Communication data rate with respect to the sensing range of distance, where the sensing scope of speed is set as $[-60, 60]$ m/s. (b) Communication data rate with respect to the sensing range of speed, where the sensing scope of distance is set as $[0, 60]$ m.

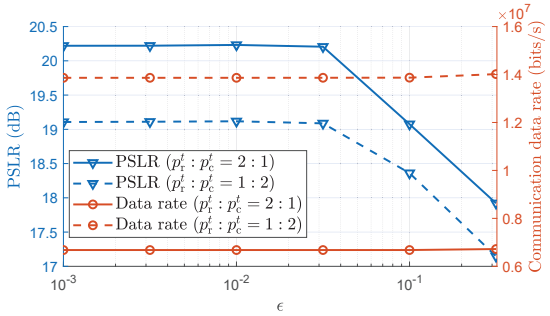

Fig. 5. PSLR and achievable data rate with respect to ϵ, where $\lambda = 0.02$ and the sensing scopes of distance and speed are set as $[0, 50]$ m and $[-60, 60]$ m/s, respectively.

Fig. 5 investigates the PSLR and the achievable data rate of the proposed cross-domain waveform design concerning ϵ, which represents the sensing power threshold in (16). As observed, the PSLR of the AF deteriorates with the increase of ϵ when $\epsilon \geq 0.03$. This phenomenon can be attributed to larger number of REs assigned for the communications including those indispensable for sensing to guarantee superior PSLR level. Conversely, when ϵ is between 0.001 and 0.1, the achievable data rate increases slightly as ϵ becomes larger, since additional communication REs may operate under unfavorable channel conditions. Therefore, we set ϵ between 0.001 and 0.03 to strike a balance in RE allocation, ensuring superior sensing and communication performances at the same time.

V. Conclusion

In this paper, a cross domain multicarrier waveform design methodology was proposed with the optimization of RE assignment and power allocation. Firstly, the AF values within the RoI of the integrated waveform were designed for a "locally" perfect AC property. The irrelevant cells outside the RoI were then optimized together with the communication power allocation for data rate enhancement in an alternating iterative manner. Numerical results showed that the proposed waveform methodology has advantages in both sensing and communication performance. Specifically, it achieves a PSLR of over 20 dB in radar sensing, while maintaining a quasi-maximum achievable data rate when sensing scopes of distance and speed are no more than 40 m and ± 50 m/s, respectively.

Acknowledgment

This work was supported in part by the National Key R&D Program of China under Grant 2021YFA0716603, in part by Young Elite Scientists Sponsorship Program by CAST under Grant 2022QNRC001, and in part by Postdoctoral Science Foundation of China under Grant 2022M720361 and 2023T160040. *(Fan Zhang and Tianqi Mao are Co-first authors with equal contribution.) (Corresponding author: Zhaocheng Wang.)*

References

[1] F. Liu, C. Masouros, A. P. Petropulu, H. Griffiths, and L. Hanzo, "Joint radar and communication design: applications, state-of-the-art, and the road ahead," *IEEE Trans. Commun.*, vol. 68, no. 6, pp. 3834–3862, Jun. 2020.

[2] H. Zhang, H. Zhang, B. Di, M. D. Renzo, Z. Han, H. V. Poor, and L. Song, "Holographic integrated sensing and communication," *IEEE J. Sel. Areas Commun.*, vol. 40, no. 7, pp. 2114–2130, Jul. 2022.

[3] F. Zhang, T. Mao, and Z. Wang, "Doppler-resilient design of CAZAC sequences for mmWave/THz sensing applications," *IEEE Trans. Veh. Technol.*, 2023, [early access].

[4] V. Petrov, G. Fodor, J. Kokkoniemi, D. Moltchanov, J. Lehtomaki, S. Andreev, Y. Koucheryavy, M. Juntti, and M. Valkama, "On unified vehicular communications and radar sensing in millimeter-wave and low terahertz bands," *IEEE Wirel. Commun.*, vol. 26, no. 3, pp. 146–153, Jun. 2019.

[5] T. Mao, J. Chen, Q. Wang, C. Han, Z. Wang, and G. K. Karagiannidis, "Waveform design for joint sensing and communications in millimeter-wave and low terahertz bands," *IEEE Trans. Commun.*, vol. 70, no. 10, pp. 7023–7039, Oct. 2022.

[6] C. Sturm and W. Wiesbeck, "Waveform design and signal processing aspects for fusion of wireless communications and radar sensing," *Proc. IEEE*, vol. 99, no. 7, pp. 1236–1259, Jul. 2011.

[7] M. Bică and V. Koivunen, "Multicarrier radar-communications waveform design for RF convergence and coexistence," in *Proc. ICASSP*, Brighton, UK, May 2019, pp. 7780–7784.

[8] C. Shi, F. Wang, S. Salous, and J. Zhou, "Joint subcarrier assignment and power allocation strategy for integrated radar and communications system based on power minimization," *IEEE Sensors J.*, vol. 19, no. 23, pp. 11 167–11 179, Dec. 2019.

[9] Y. Chen, G. Liao, Y. Liu, H. Li, and X. Liu, "Joint subcarrier and power allocation for integrated OFDM waveform in RadCom systems," *IEEE Commun. Lett.*, vol. 27, no. 1, pp. 253–257, Jan. 2023.

[10] R. W. Heath, N. González-Prelcic, S. Rangan, W. Roh, and A. M. Sayeed, "An overview of signal processing techniques for millimeter wave MIMO systems," *IEEE J. Sel. Top. Signal Process.*, vol. 10, no. 3, pp. 436–453, Apr. 2016.

[11] M. Kronauge and H. Rohling, "Fast two-dimensional CFAR procedure," *IEEE Trans. Aerosp. Electron. Syst.*, vol. 49, no. 3, pp. 1817–1823, Jul. 2013.

[12] J. Peng, G. Wei, and J. Zhu, "Power allocation method for OFDM system with both total and per-antenna power constraints," *IEEE Commun. Lett.*, vol. 12, no. 9, pp. 621–623, Sep. 2008.

[13] E. Chouzenoux and J.-C. Pesquet, "Convergence rate analysis of the majorize–minimize subspace algorithm," *IEEE Signal Process. Lett.*, vol. 23, no. 9, pp. 1284–1288, Sep. 2016.